Emergent sub-population behavior uncovered with a community dynamic metabolic model of *Escherichia coli* diauxic growth

Antonella Succurro [1,2]*, Daniel Segrè[3,4,5] and Oliver Ebenhöh [6,2]

[1] Botanical Institute, University of Cologne, Zülpicher Straße 47b, 50674 Cologne, Germany
[2] CEPLAS (Cluster of Excellence on Plant Sciences), Heinrich-Heine University, Universitätsstraße 1, 40225 Düsseldorf, Germany
[3] Bioinformatics Program and Biological Design Center, Boston University, Boston, MA, USA
[4] Department of Biology, Boston University, Boston, MA, USA
[5] Department of Biomedical Engineering, Boston University, Boston, MA, USA
[6] Institute of Quantitative and Theoretical Biology, Heinrich-Heine University, Universitätsstraße 1, 40225 Düsseldorf, Germany

* Correspondence: a.succurro@uni-koeln.de (A.S.)

Abstract

Microbial communities have adapted to greatly variable environments in order to survive both short-term perturbations and permanent changes. The diauxic shift of *Escherichia coli*, growing first on glucose and, after it is exhausted, on acetate, is still today actively studied. As a fundamental example of metabolic adaptation, we are interested in understanding if diauxie in monocultures of *E. coli* is a coordinated and uniform metabolic shift, or rather the observable emergent result of individual sub-populations behavior. To do so we first develop a modeling framework that integrates dynamic models (ordinary differential equation systems) with structural models (metabolic networks), providing an open source modeling framework that is suitable to investigate the dynamics of microbial communities. We apply our methods to model *E. coli* either as having an average, unique metabolic state or as being the combination of two *E. coli* populations adapted to one of the two carbon sources. Our results are in strong agreement with previously published data and suggest that rather than a coordinated metabolic shift, diauxie could be the emergent pattern resulting from a survival strategy where individual cells differentiate for optimal growth on different substrates in view of environmental fluctuations. This work offers a new perspective on how to use dynamic metabolic modeling to investigate population dynamics, as the proposed approach can be easily transfered to studies on other multi-species communities as well as single cells.

Importance *Escherichia coli* diauxie is a fundamental example of metabolic adaptation that has not yet been completely understood, and to this aim approaches integrating experimental and theoretical biology are needed. We present a novel dynamic metabolic modeling approach that captures diauxie as an emergent property of sub-population dynamics rather than a homogeneous metabolic shift in *E. coli* monocultures. Without fine tuning of the parameters of *E. coli* core genome-scale model we obtain good agreement with published data. Our results suggest a change of paradigm in using single organism metabolic models, which can only to a certain approximation represent the average population metabolic state. We finally provide an open source modeling framework that can be applied to model multi-organism dynamics in variable environments.

Keywords: Metabolic network modeling, Microbial communities, Diauxic growth.

1 Introduction

In natural environments microorganisms are exposed to high fluctuations of nutrient and micronutrient availability and have therefore developed adaptation strategies, both short-term to respond to temporary perturbations and long-term to increase evolutionary fitness [1]. We still miss a sound theoretical understanding of the mechanisms driving such strategies, but the recent technological advances in high-throughput experimental techniques pave the way to novel approaches integrating experimental and theoretical biology [2]. Theoretical ecology has developed over the last centuries as a solid discipline that describes ecosystems in mathematical terms as dynamic organism-environment interactions [3]. Indeed, as in statistical physics, individual behaviors in an *ensemble* result in observable emergent patterns that can be modeled with mathematical equations [4]. This is the case for the earliest models of population dynamics by Verhulst [5], Lotka [6] and Volterra [7] and for the pioneering works by Jaques Monod in modeling microbial growth [8]. With the rising academic and industrial interest in the "microbiome", systems biology approaches are becoming a new standard [9] and more methods for mathematical modeling of microbial communities are being developed [10, 11].

In constraint-based stoichiometric modeling the metabolic network model of an organism is reconstructed from its annotated genome and described mathematically as a stoichiometry matrix $\mathbf{S}$. After imposing the steady-state assumption and introducing thermodynamic and biological boundaries for the metabolic fluxes $\vec{v}$, flux balance analysis (FBA) [12, 13] defines an optimization problem in order to

identify one particular flux distribution in the solution space. As long as the objective function (which introduces further biological assumptions on the system) is linear in the fluxes, the optimization problem can be solved with linear programming (LP). FBA returns a unique solution for the objective function, but the metabolic flux distribution is in general not unique, especially in genome-scale metabolic network models (GEMs). Under the hypothesis that metabolism has evolved to make efficient use of resources and minimize waste, two specific methods were developed to extend FBA: parsimonious FBA (pFBA) [14] and minimization of metabolic adjustment (MOMA) [15]. In pFBA a second LP is defined where the value of the objective function is set to the FBA solution and the new objective is the minimization of the overall fluxes. MOMA was developed to simulate the response to the perturbation introduced by gene deletion and is based on the principle that the organism will readjust its metabolism to a minimally different configuration with respect to the wild type optima. Another extension of FBA, dynamic FBA (dFBA) [16], allows to partly recover the dynamic information lost under the steady-state assumption. In the static optimization approach (SOA) time is divided in discrete intervals and a new FBA problem is solved at time i after updating the external conditions according to the FBA solution at time $i-1$. Approaches to model microbial communities with GEMs are reviewed *e.g.* in [17].

FBA and dFBA have been applied to study one of the most basic examples of metabolic transitions: diauxie [18, 16, 19]. Discovered in the model organism *Escherichia coli* in 1941 by Monod [20, 8], diauxie is still today a topic of active research [21, 22, 23]. In aerobic conditions with glucose as sole carbon source (also generally the preferred one), *E. coli* grows secreting acetate, which it then consumes after glucose is exhausted. The molecular mechanisms driving this transition are still not completely understood and in particular it is not clear if the observed biphasic growth is the effect of a coordinated and homogeneous population shift, eventually co-regulated by memory mechanisms [24], or rather the observable behavior emerging from sub-population dynamics, as suggested *e.g.* by Solopova *et al.* for *Lactococcus lactis* [25]. In unpredictable natural environments with fluctuating nutrient availability and variable fitness landscapes, homogeneous populations have higher chances to face extinction and bet hedging becomes a selective advantage. In this work we present a study of *E. coli* diauxic growth on two carbon sources, glucose and the acetate secreted during growth on glucose, where the bacterial population is modeled either as having an average, unique metabolic state (standard FBA and dFBA approach) or as being the combination of two *E. coli* populations adapted to one of the two carbon sources. Our results suggest that rather than a coordinated metabolic shift, diauxie could be the emergent pattern resulting from a survival strategy where individual cells differentiate for optimal growth on different substrates in view of environmental fluctuations. We use a modeling approach that integrates ordinary differential equation (ODE) models with dFBA and provide an open source modeling framework that is suitable to investigate both emergent patterns from individual behavior in monocultures as well as the dynamics of multi-species communities. The simulations are first calibrated using the original dataset from Varma and Palsson, 1994 [18], and then are used to reproduce the independent set of experiments from Enjalbert *et al.*, 2015 [22]. Our results are found in agreement with these previously published data and offer a new perspective on how to use dynamic metabolic modeling to investigate population dynamics. The proposed approach can be easily transfered to studies of communities, sub-populations and also, eventually, single cells.

2 Results

We run simulations with a novel open source modeling framework developed to model ecosystem dynamics. The models are ODE systems solved with integrating routines that at each integration step solve an FBA problem. We validate the *E. coli* GEM on the data from Varma and Palsson [18] and compare two approaches for solving the FBA problem, namely parsimonious FBA (pFBA) [14] and minimization of metabolic adjustment (MOMA) [15] (Text S1). The pFBA implementation is then used to model *E. coli* diauxic shift as emergent property of sub-population dynamics on the independent data from Enjalbert *et al.* [22]. Details on the modeling approach are provided in Materials and Methods.

***E. coli* diauxie modeled with a uniform population.** A single GEM is used to model the average *E. coli* metabolic state and we compare the simulation results with the original data from Varma and Palsson [18] (Fig. S1). The parameters for the simulations are reported in Tab. 2 and 3, and the only flux constraints that we calibrate to the data are the oxygen uptake rate and the maximal acetate secretion rate. We use the same GEM model to reproduce the results from Enjalbert *et al.* [22], changing only the initial values of biomass, glucose and acetate (Fig. 1). While the pFBA simulation (Fig. 1(a)) shows a brief shift to growth on acetate at the time of glucose exhaustion (~ 4 hr), the MOMA simulation predicts a complete growth arrest already at that point, with a minimal acetate consumption to satisfy the ATP maintenance requirement implemented in the GEM (Fig. 1(b)). Both simulations well capture glucose consumption and acetate secretion, but neither of them is able to reproduce the slow acetate

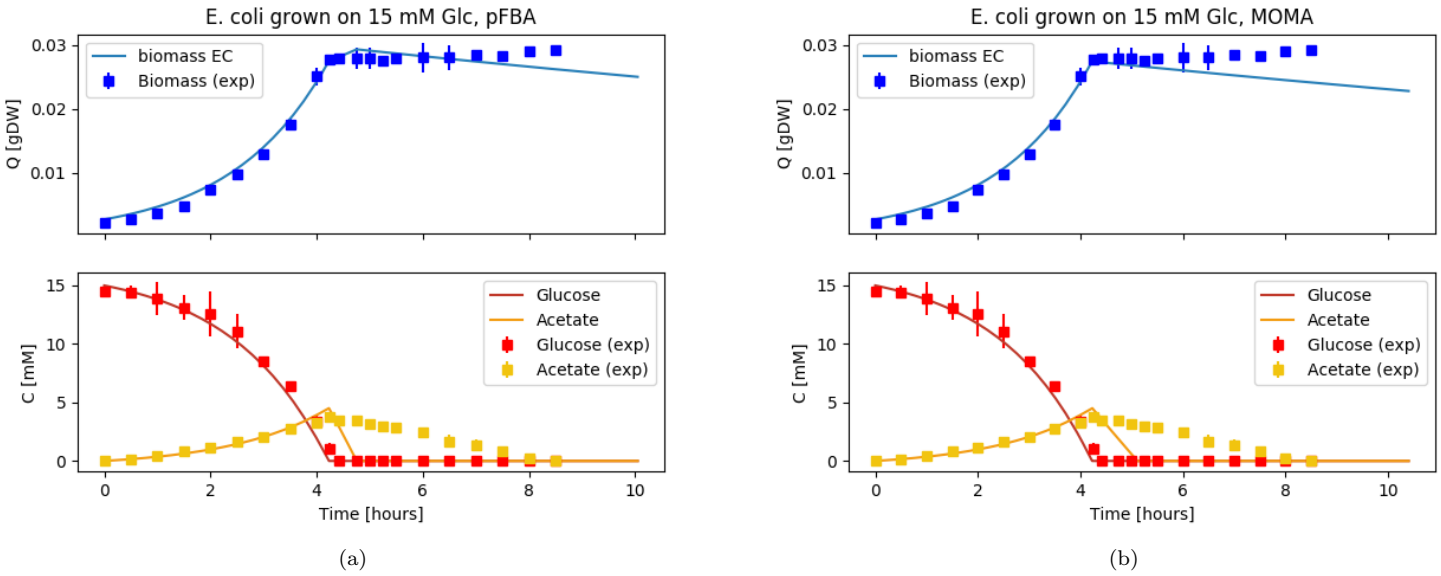

(a) (b)

Figure 1: Diauxic growth of *E. coli* modeled as a uniform population in batch conditions. Simulation (lines) is compared to data (squares) from Enjalbert *et al.* [22] as a function of time. Biomass (blue, top sub-plots), glucose and acetate (red and yellow, bottom sub-plots) are shown. The flux distribution at each time step is obtained with pFBA (a) or MOMA (b).

consumption observed experimentally. We evaluate the agreement between experiment and simulation with the R^2 distance between *in vivo* and *in silico* data for the biomass (pFBA $R^2 = 0.989$; MOMA $R^2 = 0.982$) glucose (pFBA $R^2 = 0.993$; MOMA $R^2 = 0.993$) and acetate (pFBA $R^2 = 0.277$; MOMA $R^2 = 0.409$). Tab. 1 reports the results from Enjalbert *et al.* [22] for over/under-expression of key genes associated with glucose and acetate metabolism. The same results are represented graphically in Fig. 2, where we compare the flux distributions from simulation results to these experimental findings. First, we compute the flux solutions for *E. coli* growing either on glucose or on acetate exponentially (data not shown) and compare the fluxes through the relevant reactions in *E. coli* growing on acetate with the ones in *E. coli* growing on glucose. Fig. 2(a) shows the absolute values for the flux results in the two simulations, normalized between 0 and 1 for direct comparison with the qualitative representation of the gene expression data of Tab. 1. The simulation results are consistent with the experiments, with active reactions (dark green) related to acetate consumption and anabolism (ACKr, PPCK, FBP, ICL, MALS) and inactive reactions (white) related to glycolysis (PFK, PYK) during growth on acetate, and vice-versa during growth on glucose. We then use the simulation results presented in Fig. 1 to compare the metabolic fluxes before and after glucose exhaustion (GE), *i.e.* before and after the single *E. coli* model shifts from growth on glucose to growth on acetate. Enjalbert *et al.* [22] compared the gene expression levels between samples taken at time (GE + 30 minutes) and (GE - 115 minutes). However Fig. 1 shows that according to the simulation, growth has already stopped after 30 minutes from the GE point. Indeed comparing the absolute values of fluxes taken at time (GE + 30 minutes) and (GE - 115 minutes) (Fig. S4), we observe that both pFBA and MOMA simulations qualitatively capture the down regulation trends, while neither reproduces the observed up-regulation. Fig. 2(b) shows the difference of the absolute values of fluxes taken at time (GE + 18 minutes) and (GE - 115 minutes), where in pFBA simulations growth is still observed. In this case, both simulations qualitatively capture most of the up/down regulation trends. Fig. S5 shows the metabolic network (modified from the Escher [26] map for the *E. coli* core model) with reactions of Fig. S4 highlighted and color-coded according to the gene expression data, and Fig. S6 presents the same picture but with respect to the results of Fig. 2(b).

***E. coli* diauxie modeled with a mixed population.** We use two GEMs (same parameter values as before) to model *E. coli* monoculture as a mixture of two populations, one adapted to grow on glucose and one adapted to grow on acetate. The two models EC_{Glc} and EC_{Ac} are hence constrained to uptake exclusively the respective carbon source. Two transition functions, dependent on acetate or glucose concentrations, are introduced to model cellular differentiation and shift from one population to the other (see Materials and Methods for details). We run simulations to compare different scenarios investigated experimentally by Enjalbert *et al.* [22]. Initial values of biomass, glucose and acetate are adjusted to the

Table 1: Gene expression levels reported by Enjalbert *et al.* [22]. One experiment compares *E. coli* exponentially growing on acetate with *E. coli* exponentially growing on glucose. The other experiment compares gene expression levels after glucose exhaustion (GE) with respect to 115 minutes before GE.

Gene	*acs*	*pck*	*pps*	*fbp*	*icl*	*mls*	*pfkA*	*pykF*	*ppc*	*icd*
Full growth on Acetate / Full growth on Glucose	$\Uparrow$	$\Uparrow$	$\Uparrow$	$\Uparrow$	$\Uparrow$	$\Uparrow$	$\Downarrow$	$\Downarrow$	na	na
After GE / 115 minutes before GE	$\Uparrow$	$\Uparrow$	$\sim$	$\sim$	$\sim$	$\sim$	$\Downarrow$	$\Downarrow$	$\Downarrow$	$\Downarrow$

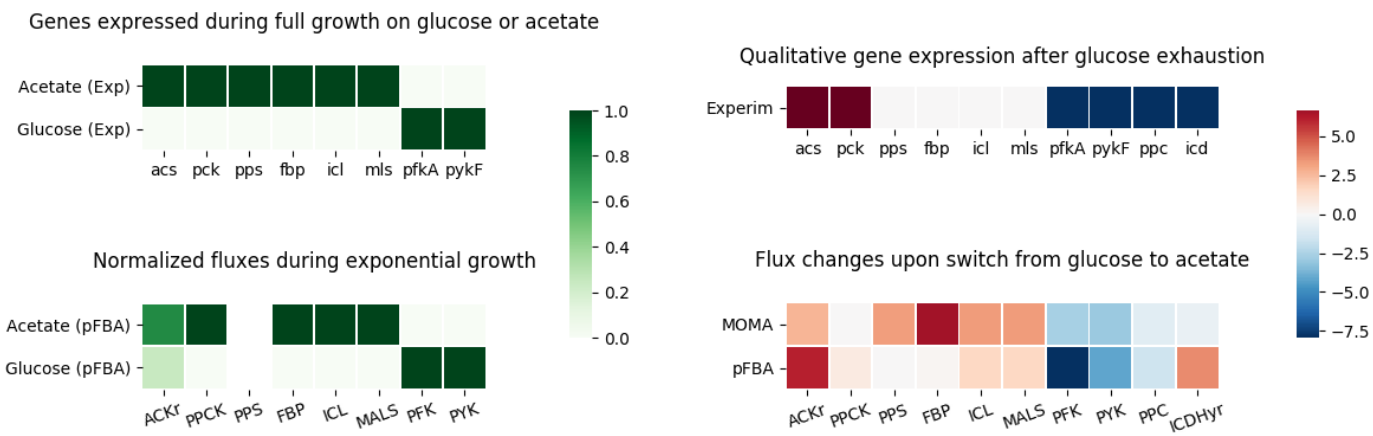

(a) (b)

Figure 2: Comparison of experimental information on gene expression levels with simulated flux distributions. The top plots represent qualitatively the gene expression data from Enjalbert *et al.* [22]. Flux solutions in the simulations for the reactions associated to the reported key genes are compared (a) between two independent simulations with *E. coli* exponentially growing either on acetate or on glucose; (b) within the same simulation (Fig. 1, growth on glucose simulated with MOMA or pFBA) before and after the point of glucose exhaustion.

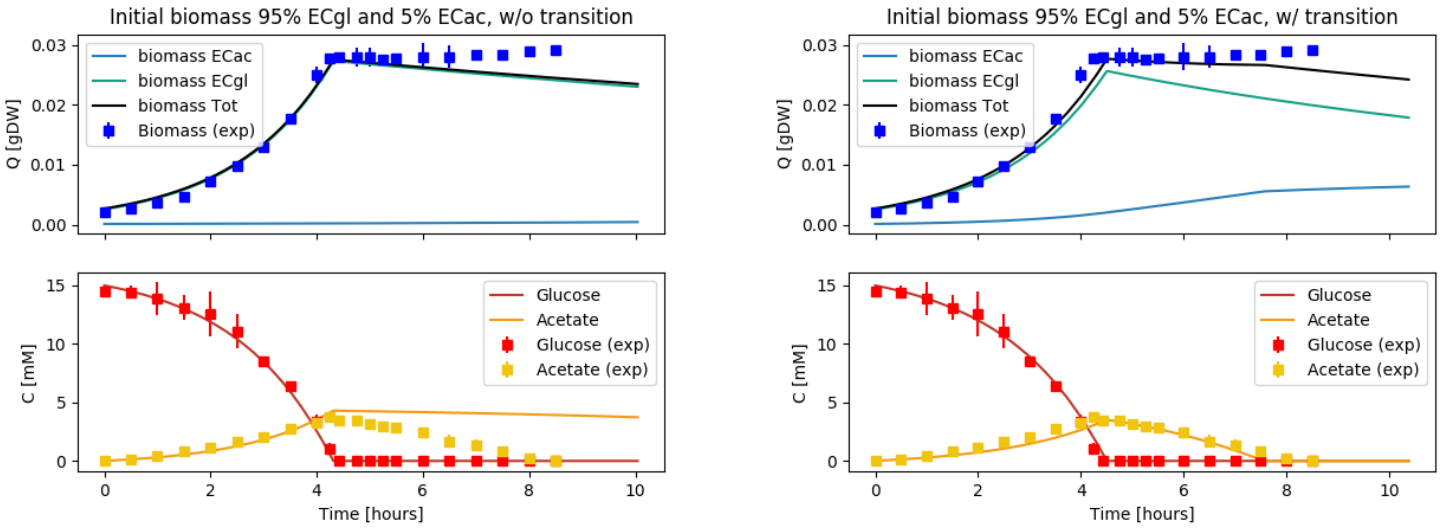

(a) (b)

Figure 3: Diauxic growth of *E. coli* modeled as a mixture of two *E. coli* populations EC_{Glc} and EC_{Ac} growing exclusively on glucose or acetate, respectively, and without (a) or with (b) possibility to shift from one population to the other. Simulation (lines) is compared to data (squares) from Enjalbert *et al.* [22] as a function of time. The upper plots show simulation results for EC_{Glc} and EC_{Ac} biomasses (light blue and aqua, respectively) and the observable *E. coli* biomass (black line simulation, blue dots data). The bottom plots show glucose and acetate (red and yellow respectively).

respective datasets. Fig. 3 shows simulations for the same condition as Fig. 1(a), with same absolute initial biomass, distributed in this case as 95% EC_{Glc} and 5% EC_{Ac}. Fig. 3(a) shows the simulation results for a scenario without transitions between the two states, whereas the results of Fig. 3(b) are obtained with active transition functions, defined here by constant transition rates as reported in Tab. 3. These transition rates, as well as the initial population ratios, were chosen following the assumption, supported by a simple mathematical model, that in constant environments the populations will converge to a constant ratio (see Text S2 for details). While both Fig. 3(a) and Fig. 3(b) well capture the biomass ($R^2 = 0.987$ and $R^2 = 0.990$, respectively) and glucose concentrations ($R^2 = 0.996$ and $R^2 = 0.997$, respectively), only the simulation including population transition can realistically reproduce the acetate consumption ($R^2 = 0.336$ and $R^2 = 0.951$ respectively), as well as a lag phase before culture crash. Neither of the two simulation however captures the eventual recovery of growth hinted by the last data points. We reproduce two other results (where only biomass measurements are available) from Enjalbert *et al.* [22], again using the same GEMs and changing only the initial conditions (biomass quantity and distribution among EC_{Glc} and EC_{Ac}) and experimental setup accordingly. By modeling the population transition with the same constant rate, we are able to explain the biomass profile in the case where *E. coli* is grown on 15 mM glucose and after glucose exhaustion the acetate concentration is maintained at around 4 mM (Fig. S11(a), $R^2 = 0.986$), but not in the case where *E. coli* is grown on 15 mM glucose and 32 mM acetate, and after glucose exhaustion the acetate concentration is maintained at the same high level (Fig. S12(a), $R^2 = 0.727$). We therefore introduce a dependency of the transition functions on the substrate concentration (see Materials and Methods for details) that well captures all the experimental scenarios (Fig. S10, S11, S12). Fig. 4(a) shows that an *E. coli* population starting with 95% EC_{Glc} and 5% EC_{Ac} well describes the biomass dynamics ($R^2 = 0.985$) and the glucose exhaustion point after around 4 h when acetate is maintained at 4 mM. Again, without fine-tuning of the GEM simulation parameters, Fig. 4(b) shows that an *E. coli* population starting with 75% EC_{Glc} and 25% EC_{Ac} reproduces the biomass measurements ($R^2 = 0.940$) and the glucose exhaustion point after around 4 h also in the experimental setup with acetate maintained at 32 mM. This initial population ratio is consistent with the range for steady state values found in the study of Text S2 for the population ratio in mixed carbon conditions.

Lag time for growth on acetate explained with population distribution. Enjalbert *et al.* [22] showed different trends in *E. coli* cultures lag time to achieve maximal growth after glucose exhaustion (GE). In their switch experiments, they sampled at different time points "mother cultures" of *E. coli* cells growing in batch conditions on 15 mM of glucose alone (M9G condition) or on 15 mM of glucose

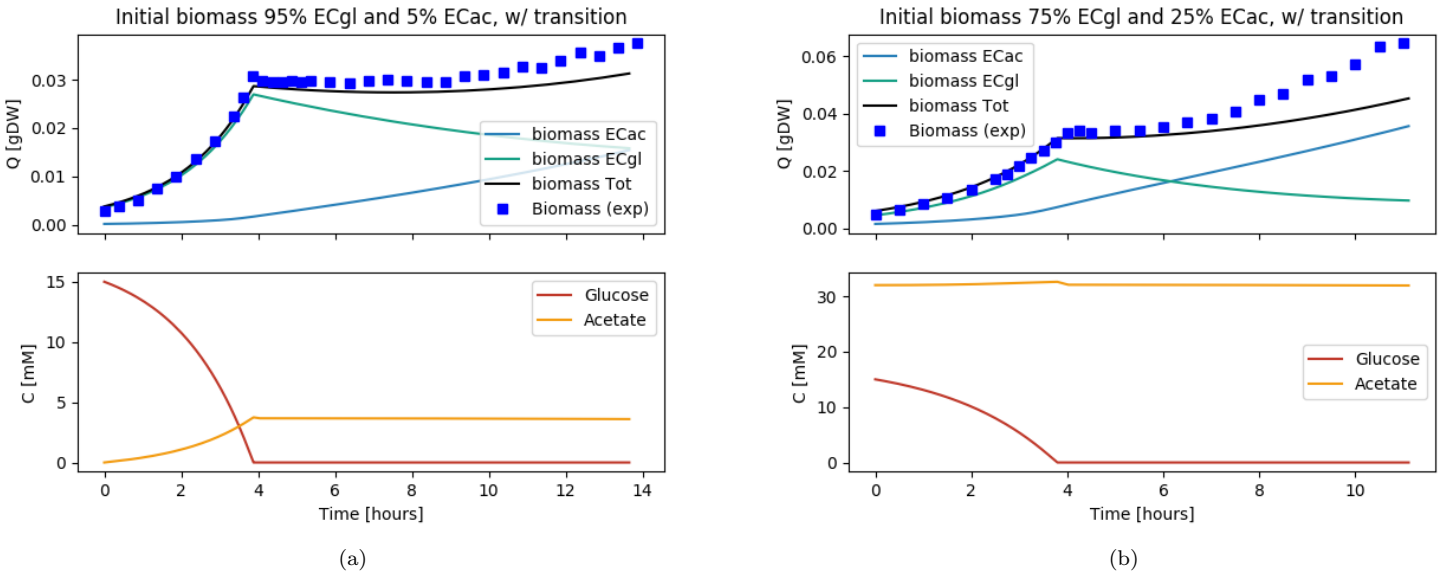

(a) (b)

Figure 4: Diauxic growth of *E. coli* modeled as a mixture of two *E. coli* populations EC_{Glc} and EC_{Ac} growing exclusively on glucose or acetate, respectively, with possibility to shift from one population to the other. (a) *E. coli* grows on 15 mM glucose and after glucose is exhausted, acetate concentration is kept at about 4 mM. (b) *E. coli* grows on 15 mM glucose and 32 mM acetate and after glucose is exhausted, acetate concentration is maintained at around that concentration. The upper plots show simulation results for EC_{Glc} and EC_{Ac} biomasses (light blue and aqua lines, respectively) and the observable *E. coli* biomass (black line simulation, blue dots data from Enjalbert *et al.* [22]). The bottom plots show simulation results for glucose and acetate (red and yellow lines respectively).

and 32mM of acetate (M9GA condition), and re-inoculated the sampled cells as "daughter cultures" into fresh media containing exclusively glucose (M9G condition) or acetate (M9A condition). We replicate this experiment *in silico* by running first simulations in the M9G and M9GA conditions. We use as M9G mother culture the simulation of the mixed EC_{Glc} and EC_{Ac} population shown in Fig. 3(b), as the experimental conditions are the same. For the M9GA mother culture we do not have an experimental dataset to refer to and we simulate a new scenario similar to the one of Fig. 4(b), with the same initial population composed of 75% EC_{Glc} and 25% EC_{Ac}, but without the feeding of additional acetate. The biomass, glucose and acetate profiles resulting from this simulation are shown in Fig. S13. The GE time point is about 4.6 hours for M9G and 3.9 hours for M9GA, consistent with the observations of Enjalbert *et al.* [22]. The *in silico* mother cultures are sampled at regular time intervals to obtain the initial biomass distribution of EC_{Glc} and EC_{Ac} for the daughter cultures and the lag time of each daughter culture is computed (see Materials and Methods for details). Fig. 5 shows the simulation results compared with the experimental data from Enjalbert *et al.* [22]. The error bars on the simulated lag time is obtained by varying the initial biomass ratio of the daughter cultures by $\pm 15\%$. Whereas a quantitative agreement between simulation and experimental results is only achieved in the M9G-M9G switch experiment (Fig. 5(a)) with the correct prediction of almost zero lag time for the daughter cells, the trend for the delay to reach maximal growth is in general qualitatively reproduced also for the other scenarios. Cultures switched from M9G to M9A (Fig. 5(a)) need, according to the simulations, about 1.5 hours before reaching maximal growth, which is more than twice the time observed experimentally. For cultures pre-grown in M9GA (Fig. 5(b)) we observe both in simulations and experiment a decreasing (increasing) lag time for daughter cultures sampled after GE for M9GA-M9A (M9GA-M9G) switches. Additional studies are reported in Text S4, in particular Fig. S14 displays the dependence of the lag time in the daughter cultures on the maximal transition values and Fig. S15 shows the same dependence, including also the distribution of the biomass ratio in the mother cultures, for a limited set of parameters.

3 Discussion

In this work we investigated a fundamental example of metabolic adaptation, namely diauxic growth of *E. coli* on glucose and acetate, with the aim of testing the following hypothesis: is diauxie in monocultures of *E. coli* the observable emergent result of individual (sub-populations) behavior? We first developed

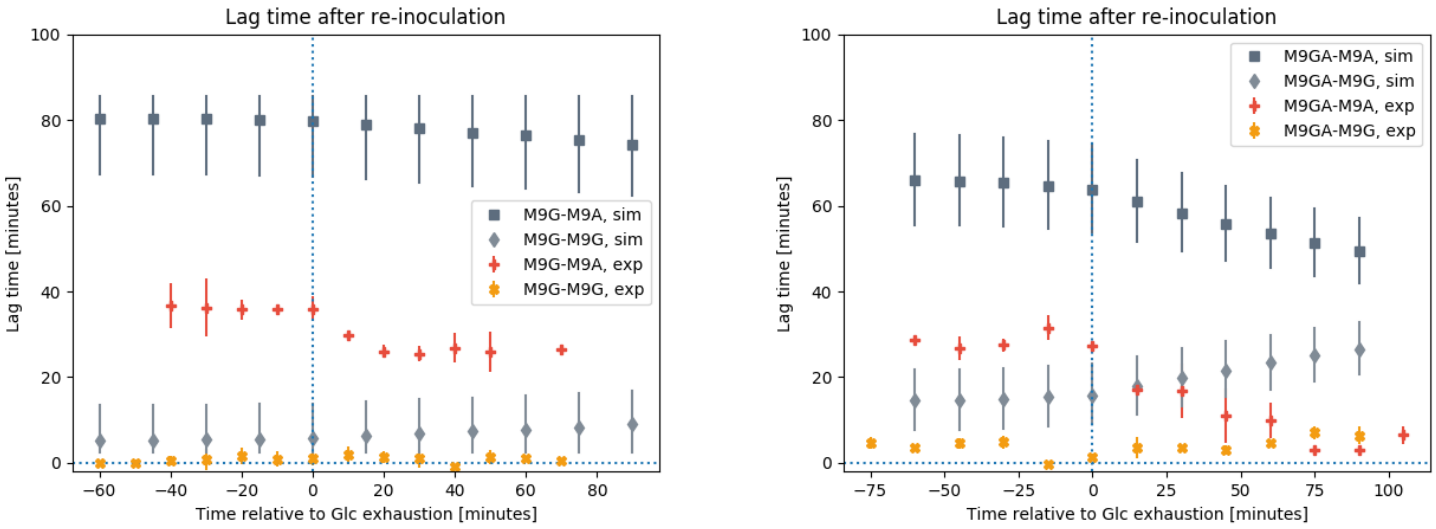

(a) (b)

Figure 5: Simulation (dark and light gray points) and experimental (orange and yellow points, data from Enjalbert *et al.* [22]) results for the delay of daughter cultures before reaching maximal growth after media switch. Mother cultures are grown either on 15 mM of glucose (M9G, (a)) or 15 mM of glucose and 32 mM of acetate (M9GA, (b)). Daughter cultures are re-inoculated into fresh media with either 15 mM of glucose (M9G, square and plus markers) or 45 mM of acetate (M9A, diamond and cross markers). The simulation error bars are obtained by varying the initial population ratios (obtained from sampling the simulated mother cultures) by $\pm 15\%$.

a modeling framework to integrate dynamic models (ODE systems) with structural models (metabolic networks) and then performed simulations to reproduce *in silico* published experimental results.

Avoiding fine-tuning of model parameters. One recurrent criticism of stoichiometric and constraint-based modeling approaches, such as FBA, is that they can be easily adjusted to reproduce experimental results by *ad hoc* changes of flux constraints. In this work we chose to take the FBA parameters mostly from experimental measurements (Tab. 2). In the case of oxygen uptake and acetate secretion, we calibrated the constraints using the results from Varma and Palsson, 1994 [18], where *E. coli* diauxic shift from glucose to acetate was first simulated with a genome scale model. Afterwards, the FBA parameters were not changed to reproduce the independent experiments from Enjalbert *et al.*, 2015 [22]. This approach to use an independent set of data for calibration of the FBA model parameters is a possible way to strengthen the confidence in subsequent results. Further model parameters of the ODE system have been chosen following reasonable hypotheses and slightly adjusted to obtain fair agreement with the experimental results, consistently among all the simulations. The initial conditions are finally specific to the experiment to reproduce.

Standard dFBA allows for abrupt metabolic readjustments. The flux distributions obtained from FBA solutions represent an average picture of the metabolic state of a population, which is in general modeled with a single genome scale model. Therefore, standard dFBA implementations where the FBA constraints evolve according to the updated external conditions, will reproduce the average change in metabolic state of the population in response to the external variations. This is equivalent to assuming that a population undergoes a coordinated, uniform metabolic shift under changing environmental conditions. Furthermore, with dFBA such transitions are, in general, abrupt. We tested two alternative approaches to simulate the diauxic shift in uniform *E. coli* monocultures, solving the FBA problems either with pFBA or with MOMA. While using pFBA was mostly equivalent to the usual dFBA implementations, by using an adaptation of MOMA we imposed that at time t_{i+1} the flux solution is minimally different from that at time t_i. This should allow for smoother metabolic adjustments to the changing external conditions. Both implementations, however, resulted in abrupt changes in the flux distributions upon the shift from glucose to acetate metabolism, therefore justifying the need of a different modeling approach.

Monocultures can be modeled as multi-sub-population systems to capture individual heterogeneity. With the introduction of two basic assumptions (first, there are two distinct metabolic states consuming either glucose or acetate; second, transition from one state to the other is driven by glucose and acetate concentrations) we were able to capture all the experimental trends published by

Enjalbert *et al.* [22]. The transitions were modeled as Hill functions of the respective substrate concentrations with a noise offset. This follows the hypothesis that there is a constant, small noise component in cell regulation, while at high concentrations of certain substrates a coordinated transition occurs, *e.g.*, if acetate is highly abundant, more cells in the glucose-consumption state will shift to the acetate-consumption state in response to the changed environment. The introduction of a transition efficiency term is a proxy for an additional contribution to cellular death rate suggested by the observation that cells can get "lost in transition" [27]. Simulation results were mostly in very good agreement with the experimental data and our results strongly support the idea, suggested also by experimental works like [28], that monocultures are an ensemble of sub-populations in different metabolic states and that environmental conditions determine which sub-population dominates. Under conditions where acetate concentrations were too low to support growth it was sufficient to model the transition as a constant random process. In contrast, in order to reproduce the data under conditions with high acetate concentrations, we had to introduce an active transition rate dependent on substrate concentrations. Interestingly, this assumption alone is sufficient to model the experimentally observed growth rate, without further fine tuning of model parameters.

The lag phase between growth on different substrates can be explained by population distributions. With standard dFBA simulations, the metabolic transition during the shift from one carbon source to another is abrupt. This is however rarely observed and, in particular, the duration of the lag phase between the exhaustion of the favored carbon source and the resumption of optimal growth on the alternate carbon source is highly variable for different environmental conditions. This observation can be easily explained as an emergent property of sub-population dynamics. Our simulations are consistent with the explanation that the delay to resume full growth actually depends on the ratio of the two sub-populations. Although the simulation results did not reproduce the experimental data quantitatively, all qualitative trends were fully explained. A number of reasons may be responsible for the observed discrepancies. For example, no experimental control of the mother cultures regarding biomass, glucose and acetate dynamics were available, to which the modeled initial population could be compared. This could lead to a bias in the later sampling and determination of sub-population ratio and therefore strongly influence the quantification of the lag time. Abrupt changes of conditions such as the re-inoculation of daughter cultures into a different media in the switch experiments might select for additional adaptation strategies. Interestingly, we observed a dramatic improvement in the quantitative agreement between experiment and simulation by relaxing the condition imposing no growth for populations inoculated on the "wrong" carbon source (Tab. S5 and Fig. S16). By allowing the glucose-consumer population sampled from glucose mother cultures to have a reduced growth on acetate, we are mimicking a situation where cells stored resources and are able to survive a bit longer (Fig. S16(a)). On the other hand, allowing a reduced growth on acetate (glucose) for the glucose-consumer (acetate-consumer) population that was exposed to both carbon sources in the mixed mother cultures, could be a proxy for a memory effect. It was indeed observed that bacterial cells show memory effects upon changes in environmental conditions [24]. To explore this potential explanation further, however, would require more systematic experiments to carefully and reproducibly determine the lag times as functions of external parameters. Finally, a recent stochastic model of the regulatory network of diauxic growth in *E. coli* suggests that the limitations of biological sensors are responsible for the lag phase [29]. From their results we can infer that in our model the transition functions, currently depending on the absolute concentration of one carbon source at a time, might not be able to capture the fine details of population shifts. A possible extension would be to introduce more complex transition mechanisms dependent on relative concentrations of primary and secondary carbon sources, a process that would need dedicated experiments for construction and validation of the new transition functions.

Outlook. There is experimental evidence that bacteria differentiate into sub-populations as a result of survival strategies [25]. Here we presented a study on a simple system with only two sub-populations growing in environments with at most two carbon sources. Our approach can be easily expanded to systems with multiple sub-populations and more complex environments. Further experiments could be designed to challenge the model hypotheses, and in particular single cell studies could allow a better definition and parameterization of the transition functions regulating the transition of cells between the sub-population. Our model assumes a simplistic rule for the transition from one population to the other, which cannot capture intermediate states. Because of this simplification, cells are modeled either in the glucose or acetate consuming state, with an instantaneous transition between these states. This simplification is both practical and plausible when we observe population dynamics as the emergent properties of individual behavior and works well in dynamically changing environments with a continuous transient. However, rather than having a well defined metabolic state, especially during the transition between states, cells might exhibit a mixed state, which could be described as a superposition of 'pure' states, much in analogy to the state vectors in quantum physics. We think that further investigations of

this novel concept of superimposed metabolic states might provide a promising new approach to study the principles of metabolic regulation.

4 Materials and Methods

FBA methods used. In stoichiometric models the stoichiometry matrix $\mathbf{S}(m \times n)$ is defined with the row and column dimensions corresponding to the numbers of metabolites m and reactions n respectively, the elements s_{ij} being the stoichiometric coefficients of metabolite i taking part in reaction j. FBA defines and solves the following LP problem:

$$\text{maximize} \quad \vec{z}, \tag{1}$$

$$\text{subject to :}$$

$$\mathbf{S}\vec{v} = 0, \tag{2}$$

$$l.b._j \leq v_j \leq u.b._j. \tag{3}$$

The steady-state assumption (Eq. 2) gives a system of equations that is under-determined and has an infinite number of solutions. Constraints on the fluxes (Eq. 3) allow to restrict the solutions to a convex solution space, which is however still infinite. The definition of an objective (Eq. 1) selects one solution, which however is in general still not unique for large (genome-scale) metabolic networks.

We consider in the following two extensions to the FBA problem definition, namely pFBA [14] and MOMA [15]. We then use these two methods to solve the FBA problem in an approach similar to dFBA [16]. Assuming that metabolism is evolved towards an efficient use of resources, pFBA finds the minimal flux distribution that returns the same objective defined by the FBA problem. We use the pFBA implementation from COBRApy [30] with maximal flux through the biomass reaction as objective function. Considering that metabolism has to respond quickly to perturbations, MOMA implements a quadratic algorithm to find the FBA solution after gene deletion that is most similar to the optimal wild type configuration. We use the MOMA implementation from COBRApy [30] in the linear approximation, with a slight modification to allow the reset of the LP problem in an iterative way, necessary to run MOMA within the dFBA approach. Indeed, the MOMA solution obtained at time t_i is used to compute the MOMA solution at time t_{i+1} as the minimally different solution that satisfies the objective function. Also here the objective function is maximal flux through the biomass reaction.

Modeling framework integrating ODE and FBA. In the SOA of dFBA the boundary conditions in Eq. 3 are updated at discrete time steps according to the solution of the FBA problem in the previous time interval. Assuming quasi-steady-state conditions, *i.e.* that metabolism readjustments are faster than external environmental changes, dFBA can approximate the dynamic response of a GEM to a changing environment. Our approach is an extension of dFBA. The model is built as a system of ODEs, whose dimension depends on the dynamics to be modeled. Each ODE describes the variation in time of either an organism's biomass, metabolites, or other regulatory/dynamic processes. The biomasses and the metabolites can, but don't have to, correspond to the respective variables in a GEM. Their ODEs vary according to a function that can then depend on the flux solutions $\vec{v}$

$$\frac{dq_i}{dt} = \mathcal{F}(\vec{p}; \vec{v}, \vec{q}, t). \tag{4}$$

The ODE system is then solved with integrating routines with automated choice of time step. Each integration step solves the FBA problem (or pFBA, or MOMA) to obtain the current reaction rates for Eq 4, updates the metabolite quantities according to the FBA solution, re-computes the flux boundaries of Eq. 3 according to specific reaction kinetics (typically Michaelis-Menten enzyme kinetics), and re-defines the FBA problems with the new boundaries and/or other regulatory mechanisms defined by the user.

The modeling framework is written in Python (Python Software Foundation, `https://www.python.org/`) following the object-oriented programming (OOP) paradigm for efficiency and flexibility of use. The framework uses functionality from the following third-party packages: numpy [31], scipy [32], matplotlib [33], COBRApy [30], pandas [34]. In particular, we use COBRApy methods to solve the FBA problems and python integrators from the `scipy.integrate` method `ode` to solve the system of ordinary differential equations.

***E. coli* uniform population model.** The GEM of *E. coli* used is the core model from [35] downloaded from `http://bigg.ucsd.edu/models/e_coli_core`. The *E. coli* model EC_{any} is constrained on the consumption of "any" carbon sources (glucose, Gl, or acetate, Ac) solely by the environmental conditions, and the lower bound of the exchange reactions (EX_Glc_e and EX_Ac_e respectively) follows two

simple Michaelis-Menten kinetics

$$l.b._{\text{EX_Glc_e}}^{\text{EC}_{\text{any}}} = -V_M^{\text{Gl}} \frac{[\text{Gl}]}{[\text{Gl}] + K_M^{\text{Gl}}}, \tag{5}$$

$$l.b._{\text{EX_Ac_e}}^{\text{EC}_{\text{any}}} = -V_M^{\text{Ac}} \frac{[\text{Ac}]}{[\text{Ac}] + K_M^{\text{Ac}}}. \tag{6}$$

The ODE system is defined as

$$\frac{d\text{BM}_{\text{EC}_{\text{any}}}}{dt} = v_\mu^{\text{EC}_{\text{any}}} \cdot \text{BM}_{\text{EC}_{\text{any}}} - \delta \text{BM}_{\text{EC}_{\text{any}}}, \tag{7}$$

$$\frac{d\text{Gl}}{dt} = v_{\text{EX_Glc_e}}^{\text{EC}_{\text{any}}} \cdot \text{BM}_{\text{EC}_{\text{any}}} + \xi_{\text{fed-batch}}, \tag{8}$$

$$\frac{d\text{Ac}}{dt} = v_{\text{EX_Ac_e}}^{\text{EC}_{\text{any}}} \cdot \text{BM}_{\text{EC}_{\text{any}}}, \tag{9}$$

where v_μ is the reaction rate of the biomass function (proxy for growth rate) in the FBA model, δ is the cell death rate and $\xi_{\text{fed-batch}}$ is a positive rate in fed-batch conditions and zero in batch conditions. Parameters and initial conditions are reported in Table 3. Either pFBA or MOMA are used to solve the FBA problem.

***E. coli* mixed population model.** Two *E. coli* core models are loaded and defined as either Glucose consumer (EC_{Glc}) or Acetate consumer (EC_{Ac}) by switching off uptake of the other carbon source

$$l.b._{\text{EX_Glc_e}}^{\text{EC}_{\text{Glc}}} = -V_M^{\text{Gl}} \frac{[\text{Gl}]}{[\text{Gl}] + K_M^{\text{Gl}}}, \tag{10}$$

$$l.b._{\text{EX_Glc_e}}^{\text{EC}_{\text{Ac}}} = 0, \tag{11}$$

$$l.b._{\text{EX_Ac_e}}^{\text{EC}_{\text{Glc}}} = 0, \tag{12}$$

$$l.b._{\text{EX_Ac_e}}^{\text{EC}_{\text{Ac}}} = -V_M^{\text{Ac}} \frac{[\text{Ac}]}{[\text{Ac}] + K_M^{\text{Ac}}}. \tag{13}$$

The ODE system is defined as

$$\frac{d\text{BM}_{\text{EC}_{\text{Glc}}}}{dt} = (v_\mu^{\text{EC}_{\text{Glc}}} - \psi - \delta) \cdot \text{BM}_{\text{EC}_{\text{Glc}}} + \varepsilon\phi \text{BM}_{\text{EC}_{\text{Ac}}}, \tag{14}$$

$$\frac{d\text{BM}_{\text{EC}_{\text{Ac}}}}{dt} = (v_\mu^{\text{EC}_{\text{Ac}}} - \phi - \delta) \cdot \text{BM}_{\text{EC}_{\text{Ac}}} + \varepsilon\psi \text{BM}_{\text{EC}_{\text{Glc}}}, \tag{15}$$

$$\frac{d\text{Gl}}{dt} = v_{\text{EX_Glc_e}}^{\text{EC}_{\text{Glc}}} \cdot \text{BM}_{\text{EC}_{\text{Glc}}} + v_{\text{EX_Glc_e}}^{\text{EC}_{\text{Ac}}} \cdot \text{BM}_{\text{EC}_{\text{Ac}}} + \xi_{\text{fed-batch}}, \tag{16}$$

$$\frac{d\text{Ac}}{dt} = v_{\text{EX_Ac_e}}^{\text{EC}_{\text{Glc}}} \cdot \text{BM}_{\text{EC}_{\text{Glc}}} + (v_{\text{EX_Glc_e}}^{\text{EC}_{\text{Ac}}} + \zeta \cdot H(t - t_x)) \cdot \text{BM}_{\text{EC}_{\text{Ac}}}, \tag{17}$$

where $\zeta \cdot H(t - t_x)$ is a Heaviside function activated at the time t_x of glucose exhaustion in order to keep acetate constant, and ψ and ϕ are functions that model the cellular shift from EC_{Glc} to EC_{Ac} and EC_{Ac} to EC_{Glc}, respectively, and $0 < \varepsilon < 1$ is a positive factor representing the transition efficiency. The functions ψ and ϕ are modeled as Hill functions with a noise offset

$$\psi([\text{Ac}]) = \psi_0 + V_M^\psi \frac{[\text{Ac}]^5}{[\text{Ac}]^5 + K_M^{\psi\ 5}}, \tag{18}$$

$$\phi([\text{Gl}]) = \phi_0 + V_M^\phi \frac{[\text{Gl}]^5}{[\text{Gl}]^5 + K_M^{\phi\ 5}}, \tag{19}$$

and for $V_M^\phi = V_M^\psi = 0$ they are constant transition rates. Parameters and initial conditions are reported in Table 3. For mixed population simulations, pFBA is used to solve the FBA problem.

Switch experiment simulations. Two *E. coli* mixed population model simulations are run as "mother cultures" as shown in Table 3 for "M9G" and "M9GA" conditions (glucose and glucose plus acetate, respectively). From each mother culture we sample 11 time points between -1 and +1.5 hours from the respective GE time (4.6 hours for M9G and 3.9 hours M9GA) to obtain the biomass ratio between EC_{Glc} and EC_{Ac} to be used as initial condition for the re-inoculation simulations. The percentage of EC_{Glc} biomass at these time points is reported in Table 4. The "daughter cultures" are then grown either in "M9G" or "M9A" conditions (glucose and acetate only, respectively; see Table 3). A total of 44

Table 2: Fixed parameters for all simulations. The death rate δ is computed assuming a cell death of 1% per generation (Saint-Ruf *et al.*, 2004 [36]) and a generation time of 20 minutes. The Michaelis-Menten parameters for substrate uptake are taken from Gosset, 2005 [37]. These parameters are also used in previously published dFBA implementations [38].

	L.B. EX_O2 $\frac{\text{mmol}}{\text{gDW hr}}$	$\boldsymbol{\delta}$ hr^{-1}	$\mathbf{V_M^{Glc}}$ $\frac{\text{mmol}}{\text{gDW hr}}$	$\mathbf{K_M^{Glc}}$ mM	$\mathbf{V_M^{Ac}}$ $\frac{\text{mmol}}{\text{gDW hr}}$	$\mathbf{K_M^{Ac}}$ mM
Value	-10.	0.03	10.0	0.01	10.0	0.01

Table 3: Parameters of the simulations.

	BM(0) 10^{-3} gDW	$\left.\frac{\mathbf{EC_{Glc}}}{\mathbf{EC_{Ac}}}\right\|_{\mathbf{0}}$	**Glc(0)** mmol	**Ac(0)** mmol	$\boldsymbol{\xi}$ $\frac{\text{mmol}}{\text{hr}}$	$\boldsymbol{\zeta}$ $\frac{\text{mmol}}{\text{hr}}$	t_x hr	ψ_0 hr^{-1}	$\mathbf{V_M^{\psi}}$ hr^{-1}	$\mathbf{K_M^{\psi}}$ mM	ϕ_0 hr^{-1}	$\mathbf{V_M^{\phi}}$ hr^{-1}	$\mathbf{K_M^{\phi}}$ mM	$\boldsymbol{\varepsilon}$
Fig. S1(a), S1(c)	0.3	NA	10.8	0.4	0.0	0.0	0.0	0.0	0.0	0.0	0.0	0.0	0.0	0.0
Fig. S1(b), S1(d)	0.24	NA	0.82	0.1	1.1	0.0	0.0	0.0	0.0	0.0	0.0	0.0	0.0	0.0
Fig. 1(a), 1(b)	2.7	NA	15.0	0.0	0.0	0.0	0.0	0.0	0.0	0.0	0.0	0.0	0.0	0.0
Fig. 3(a)	2.7	$\frac{0.95}{0.05}$	15.0	0.0	0.0	0.0	0.0	0.0	0.0	0.0	0.0	0.0	0.0	0.0
Fig. 3(b), S10(a)	2.7	$\frac{0.95}{0.05}$	15.0	0.0	0.0	0.0	0.0	0.04	0.0	0.0	0.04	0.0	0.0	0.9
Fig. S10(b)	2.7	$\frac{0.95}{0.05}$	15.0	0.0	0.0	0.0	0.0	0.04	0.2	30.0	0.04	0.2	5.0	0.9
Fig. S11(a)	3.8	$\frac{0.75}{0.25}$	15.0	0.0	0.0	9.1	4.0	0.04	0.0	0.0	0.04	0.0	0.0	0.9
Fig. 4(a), S11(b)	3.8	$\frac{0.75}{0.25}$	15.0	0.0	0.0	9.1	4.0	0.04	0.2	30.0	0.04	0.2	5.0	0.9
Fig. S12(a)	6.0	$\frac{0.75}{0.25}$	15.0	32.0	0.0	9.1	4.0	0.04	0.0	0.0	0.04	0.0	0.0	0.9
Fig. 4(b), S12(b)	6.0	$\frac{0.75}{0.25}$	15.0	32.0	0.0	9.1	4.0	0.04	0.2	30.0	0.04	0.2	5.0	0.9
M9G (m.c.)	2.7	$\frac{0.95}{0.05}$	15.0	0.0	0.0	0.0	0.0	0.04	0.2	30.0	0.04	0.2	5.0	0.9
M9GA (m.c.)	6.0	$\frac{0.75}{0.25}$	15.0	32.0	0.0	0.0	0.0	0.04	0.2	30.0	0.04	0.2	5.0	0.9

Table 4: Percentage of EC_{Glc} biomass in M9G and M9GA conditions at time points relative to glucose exhaustion, in hours.

	-1.0	**-0.75**	**-0.5**	**-0.25**	**0**	**0.25**	**0.5**	**0.75**	**1.0**	**1.25**	**1.5**
M9G	95.1	95.0	94.8	94.5	94.3	93.2	92.3	91.4	90.6	89.4	88.2
M9GA	78.7	78.6	78.1	77.3	76.5	73.2	70.1	67.2	64.5	62.0	59.7

simplified simulations (see Text S4) are hence run, 11 for each of the following 4 switch experiments: M9G to M9G; M9G to M9A; M9GA to M9G; M9GA to M9A. For each simulation, the lag time is computed according to Enjalbert *et al.* [22]:

$$t_{\text{lag}} = t_1 - \frac{\ln(X_1/X_0)}{\mu_{\max}} \tag{20}$$

where X_0 is the total initial *E. coli* biomass, X_1 is the total *E. coli* biomass value at time t_1 (chosen as 1.5 hours as in [22]), and $\mu_{\max}$ are taken as the values reported in Enjalbert *et al.* [22].

Published experimental data. Experimental data (values with standard deviations, when available) from the publication [22] were kindly provided by Prof. Enjalbert. The data from [18] were extracted from the publication's figures using WebPlotDigitizer [39].

Availability of data and materials. The version v1.0 of the modeling framework used to obtain the results presented in this manuscript is publicly available with instructions to install and run simulations at `https://github.com/QTB-HHU/dfba-ode-framework_ecoli-diauxie`. The development version is hosted on `https://gitlab.com/asuccurro/dfba-ode-framework` and people interested in contributing can request access by contacting the corresponding author (A.S.).

5 Supplemental Material

Supplemental material for this article may be found at `xxx`

TEXT S1, FIGURE S1, S2, S3, PDF file, 809 KB.
FIGURE S4 PNG file, 17 KB.
FIGURE S5 EPS file, 2.3 MB.
FIGURE S6 EPS file, 2.3 MB.
TEXT S2, FIGURE S7, S8, S9, TABLE S1, S2, PDF file, 490 KB.
TEXT S3, FIGURE S10, S11, S12, TABLE S3, PDF file, 558 KB.
TEXT S4, FIGURE S13, S14, S15, S16, TABLE S4, S5, PDF file, 486 KB.

6 Acknowledgments

A.S., D.S. and O.E. initiated and designed the project; A.S. developed the modeling framework, performed simulations and wrote the initial manuscript; all authors contributed to the interpretation of the results and to the final manuscript. The authors are grateful to Prof. Brice Enjalbert for kindly providing the experimental data used to compare with the simulation results. A.S. and O.E. are supported by the Deutsche Forschungsgemeinschaft, Cluster of Excellence on Plant Sciences CEPLAS (EXC 1028). A.S. was supported also by funding from the European Commission Seventh Framework Marie Curie Initial Training Network project 'AccliPhot' (grant agreement number PITN-GA-2012-316427). D.S. acknowledges funding from the U.S. Department of Energy (DE-SC0012627), the NIH (5R01DE024468, R01GM121950), the National Science Foundation (Grants 1457695, NSFOCE-BSF 1635070), the MURI Grant W911NF-12-1-0390, the Human Frontiers Science Program (RGP0020/2016), and the Boston University Interdisciplinary Biomedical Research Office. The funders had no role in study design, data collection and interpretation, or the decision to submit the work for publication.

References

[1] Coco van Boxtel, et al. Taking chances and making mistakes: non-genetic phenotypic heterogeneity and its consequences for surviving in dynamic environments. *J R Soc Interface*, 14(132):20170141, jul 2017.

[2] Antonella Succurro, Fiona Wanjiku Moejes, and Oliver Ebenhöh. A Diverse Community To Study Communities: Integration of Experiments and Mathematical Models To Study Microbial Consortia. *J Bacteriol*, 199(15):e00865–16, aug 2017.

[3] J. D. Murray. *Mathematical Biology*, volume 17 of *Interdisciplinary Applied Mathematics*. Springer New York, New York, NY, 2004.

[4] George I Hagstrom and Simon A Levin. Marine Ecosystems as Complex Adaptive Systems: Emergent Patterns, Critical Transitions, and Public Goods. *Ecosystems*, 20(3):458–476, apr 2017.

[5] Pierre-François Verhulst. Notice sur la loi que la population poursuit dans son accroissement. *Corresp mathématique Phys*, 10:113–121, 1838.

[6] AJ Lotka. *Elements of Physical Biology*. Baltimore (MD), 1925.

[7] V Volterra. Fluctuations in the Abundance of a Species considered Mathematically. *Nature*, 118:558–560, oct 1926.

[8] J Monod. The Growth of Bacterial Cultures. *Annu Rev Microbiol*, 3(1):371–394, oct 1949.

[9] Stefanie Widder, et al. Challenges in microbial ecology: building predictive understanding of community function and dynamics. *ISME J*, 10(11):2557–2568, nov 2016.

[10] Hyun-Seob Song, et al. Mathematical Modeling of Microbial Community Dynamics: A Methodological Review. *Processes*, 2(4):711–752, oct 2014.

[11] Ali R Zomorrodi and Daniel Segrè. Synthetic Ecology of Microbes: Mathematical Models and Applications. *J Mol Biol*, 428(5):837—-861, nov 2015.

[12] David A. Fell and J R Small. Fat synthesis in adipose tissue. An examination of stoichiometric constraints. *Biochem J*, 238(3):781–786, sep 1986.

[13] Amit Varma and Bernhard O. Palsson. Metabolic Capabilities of Escherichia coli II. Optimal Growth Patterns. *J Theor Biol*, 165(4):503–522, dec 1993.

[14] Nathan E Lewis, et al. Omic data from evolved E. coli are consistent with computed optimal growth from genome-scale models. *Mol Syst Biol*, 6, jul 2010.

[15] Daniel Segrè, Dennis Vitkup, and George M Church. Analysis of optimality in natural and perturbed metabolic networks. *Proc Natl Acad Sci U S A*, 99(23):15112–7, nov 2002.

[16] Radhakrishnan Mahadevan, Jeremy S Edwards, and Francis J Doyle. Dynamic flux balance analysis of diauxic growth in Escherichia coli. *Biophys J*, 83(3):1331–1340, sep 2002.

[17] Antonella Succurro and Oliver Ebenhöh. Review and perspective on mathematical modeling of microbial ecosystems. *Biochem Soc Trans*, page BST20170265, mar 2018.

[18] A Varma and B O Palsson. Stoichiometric flux balance models quantitatively predict growth and metabolic by-product secretion in wild-type Escherichia coli W3110. *Appl Environ Microbiol*, 60(10):3724–3731, oct 1994.

[19] William R. Harcombe, et al. The Ability of Flux Balance Analysis to Predict Evolution of Central Metabolism Scales with the Initial Distance to the Optimum. *PLoS Comput Biol*, 9(6):e1003091, jun 2013.

[20] Jacques. Monod. *Recherches sur la croissance des cultures bactèriennes*. Hermann & cie, Paris, 1942.

[21] Sarah Boulineau, et al. Single-Cell Dynamics Reveals Sustained Growth during Diauxic Shifts. *PLoS One*, 8(4):e61686, apr 2013.

[22] Brice Enjalbert, et al. Acetate Exposure Determines the Diauxic Behavior of Escherichia coli during the Glucose-Acetate Transition. *J Bacteriol*, 197(19):3173–81, oct 2015.

[23] Troy E Sandberg, et al. Laboratory Evolution to Alternating Substrate Environments Yields Distinct Phenotypic and Genetic Adaptive Strategies. *Appl Environ Microbiol*, 83(13):e00410–17, jul 2017.

[24] Guillaume Lambert and Edo Kussel. Memory and Fitness Optimization of Bacteria under Fluctuating Environments. *PLoS Genet*, 10(9):e1004556, sep 2014.

[25] Ana Solopova, et al. Bet-hedging during bacterial diauxic shift. *Proc Natl Acad Sci U S A*, 111(20):7427–32, may 2014.

[26] Zachary A. King, et al. Escher: A Web Application for Building, Sharing, and Embedding Data-Rich Visualizations of Biological Pathways. *PLOS Comput Biol*, 11(8):e1004321, aug 2015.

[27] Johan H van Heerden, et al. Lost in transition: start-up of glycolysis yields subpopulations of nongrowing cells. *Science*, 343(6174):1245114, feb 2014.

[28] Christine M. DeGennaro, Yonatan Savir, and Michael Springer. Identifying Metabolic Subpopulations from Population Level Mass Spectrometry. *PLoS One*, 11(3):e0151659, mar 2016.

[29] Dominique Chu. Limited by sensing - A minimal stochastic model of the lag-phase during diauxic growth. *J Theor Biol*, 414:137–146, feb 2017.

[30] Ali Ebrahim, et al. COBRApy: COnstraints-Based Reconstruction and Analysis for Python. *BMC Syst Biol*, 7(1):74, jan 2013.

[31] Stefan van der Walt, S Chris Colbert, and Gael Varoquaux. The NumPy Array: A Structure for Efficient Numerical Computation. *Comput Sci Eng*, 13(2):22–30, mar 2011.

[32] Eric Jones, Travis Oliphant, and Pearu Peterson. SciPy: Open source scientific tools for Python. *http://www.scipy.org/*, 2001.

[33] John D. Hunter. Matplotlib: A 2D Graphics Environment. *Comput Sci Eng*, 9(3):90–95, 2007.

[34] Wes McKinney. pandas: a Foundational Python Library for Data Analysis and Statistics. *http://pandas.sourceforge.net/*, 2011.

[35] Jeffrey D. Orth, Bernhard Ø. Palsson, and R. M. T. Fleming. Reconstruction and Use of Microbial Metabolic Networks: the Core Escherichia coli Metabolic Model as an Educational Guide. *EcoSal Plus*, 4(1), sep 2010.

[36] Claude Saint-Ruf, François Taddei, and Ivan Matic. Stress and survival of aging Escherichia coli rpoS colonies. *Genetics*, 168(1):541–6, sep 2004.

[37] Guillermo Gosset. Improvement of Escherichia coli production strains by modification of the phosphoenolpyruvate:sugar phosphotransferase system. *Microb Cell Fact*, 4(1):14, may 2005.

[38] William R Harcombe, et al. Metabolic resource allocation in individual microbes determines ecosystem interactions and spatial dynamics. *Cell Rep*, 7(4):1104–1115, may 2014.

[39] Ankit Rohatgi. Webplotdigitizer v4.0, 2017. [Online; accessed 10-January-2018].